Design, modeling and performance monitoring of a photovoltaic–thermal (PVT) water collector

Niccolò Aste, Fabrizio Leonforte *, Claudio Del Pero

Architecture, Built Environment and Construction Engineering A.B.C., Politecnico di Milano, Via Bonardi 9, 20133 Milano, Italy

Received 21 February 2014; received in revised form 4 August 2014; accepted 22 November 2014
Available online 15 December 2014

1. Introduction

PV technology is able to convert solar radiation in electricity with an efficiency ranging from 5% to 25%, meaning that a significant part of the incident solar energy is reflected or converted in thermal energy. This leads to an increase in the PV cells working temperature and, consequently, a drop of electricity conversion efficiency. For that reason, over the years, many research efforts have been spent on the development of hybrid photovoltaic–thermal (PVT) technology (water or air heat-transfer fluid) which is able to produce electricity and thermal energy at the same time (Aste et al., 2008; Chow, 2010) with better overall performances of the two separated systems (i.e. thermal and photovoltaic) (Van Helden et al., 2004).

* Corresponding author. Tel.: +39 0223999468; fax: +39 0223999469.
E-mail address: fabrizio.leonforte@polimi.it (F. Leonforte).

The most investigated PVT technology in recent time is based on systems using water as heat transfer fluid, because they achieve higher overall efficiencies than air systems (Herrando et al., 2014) due to higher heat capacity of water, so the system can be used during the whole year. PVT modules can also be classified depending on the pres-ence or absence of the air gap formed between the trans-parent frontal cover and the absorber. The two types of PVT collector are called "covered" and "uncovered". In uncovered collectors, the absorber is in direct contact with the environment, so the heat losses are considerable and the fluid temperatures are very influenced by external parameters (e.g. ambient temperature, wind speed, etc.).

For these reasons, it is generally more convenient to adopt covered collector, whose goal is to transmit the greatest part of thermal fraction of the incident solar radiation to the absorber surface, restricting convection and radiation losses, in order to achieve higher energy and exer-

Nomenclature

AM	Air Mass (–)
β	thermal expansion coefficient (K^{-1})
C_G	glass cover heat capacity (J/kg K)
C_w	heat capacity of the heat transfer fluid (J/kg K)
h_v	external convective heat transfer coefficient (W/m^2 K)
h_e	external radiative + convective heat transfer coefficient (W/m^2 K)
h_{ic}	convective heat transfer coefficient of the air in the gap (W/m^2 K)
h_{rG-PV}	radiative heat transfer coefficient between glass and PV sandwich (W/m^2 K)
h_{rG-sky}	external radiative heat transfer coefficient between glass cover and sky (W/m^2 K)
h_w	heat transfer coefficient of heat exchanger (W/m^2 K)
E	electricity generated in DC during a day (W h/m^2 day)
H	air gap thickness (m)
F	sky view factor of the collector (–)
g	gravity acceleration (m/s^2)
G	daily solar irradiation on module plane (W h/m^2 day)
I_t	solar irradiance on the collector (W/m^2)
I_{mpp}	current at maximum power point (A)
I_{sc}	short circuit current (A)
L	length of the channel (m)
k_α	absorption correction factor of PV efficiency (–)
k_γ	temperature correction factor of PV efficiency (–)
k_θ	optical correction factor of PV efficiency (–)
k_λ	spectrum correction factor of PV efficiency (–)
k_g	low irradiance correction factor of PV efficiency (–)
$\dot{m}$	flow rate (kg/s)
M_w	mass fluid in storage tank (kg)
n	number of channels (–)
N	sky cloud coverage in octaves (–)
Nu	Nusselt number (–)
p	packing factor (–)
P_n	nominal power of the PV module (W)
P_i	output power generated by the PV module (W)
PR_d	daily performance ratio (%)
PR_i	performance ratio on power (%)
Ra	Raleigh number (–)
S_G	area of the glass cover (m^2)
S_{PV-a}	area of the PV absorber (m^2)
S_S	cross section area of an absorber channel (m^2)
S_{tk}	external area of the storage tank (m^2)
t	time (s)
T_e	ambient temperature (K)
T_G	glass cover temperature (K)
T_{ma}	mean air gap temperature (K)
T_{mf}	mean temperature of the water in the absorber (K)
T_{PV}	PV cell temperature (K)
T_{in}	inlet fluid temperature from the collector (K)
T_{tk}	mean fluid temperature of the storage tank (K)
T_{out}	outlet fluid temperature from the collector (K)
T_{G-sky}	average glass cover–sky temperature (K)
U_F	lateral and back heat loss coefficient of the collector (W/m^2 K)
U_{tk}	heat loss coefficient of the storage tank (W/m^2 K)
V_{mpp}	voltage at maximum power point (V)
V_{oc}	open circuit voltage (V)
Vw_e	wind velocity (m/s)
α_G	solar absorbance of the glass cover (–)
α_{PV}	solar absorbance of PV cells (–)
γ_{PV}	temperature coefficient on power of the PV cells (%/K)
δ_G	glass cover thickness (m)
δ_{PV}	PV sandwich thickness (m)
ε_G	infrared emissivity of the glass cover (–)
ε_{G-PV}	equivalent glass-absorber infrared emissivity (–)
ε_{PV}	infrared emissivity of the PV cells (–)
θ	tilt angle of the collector (°)
λ	air thermal conductivity (W/m K)
η_a	actual efficiency of the PV sandwich (%)
η_n	nominal efficiency of the PV sandwich (%)
η_{PES}	primary energy saving efficiency (–)
η_{th}	thermal efficiency of the PVT collector (–)
η_{Tpower}	average efficiency of power plants at national level (–)
ν	kinematic viscosity of air (m^2/s)
ρ_G	glass cover density (kg/m^3)
ρ_{PV}	PV sandwich density (kg/m^3)
ρ_w	water density (kg/m^3)
σ	Stefan–Boltzmann constant ($W/m^2 K^4$)
τ_n	solar transmittance of the glass cover, at normal incident angle (–)
τ_G	solar transmittance of the glass cover (–)
φ	thermal diffusivity of air (m^2/s)

gy performance than uncovered systems, estimated between 10% and 30% (Fraisse et al., 2007; Chow et al., 2009).

For such reasons, the present work focuses on the design and realization of an experimental PVT water collector built with thin film PV technology and a roll-bond flat plate absorber. Moreover, despite numerous PVT prediction tools exists, because none of them takes into account all the factors and the losses that are involved in the energy balance of an hybrid collector system, such as spectral

efficiency of PV cells or radiative heat exchange between PV module and sky, a mathematical simulation model was developed to evaluate the performances of the designed collector; finally, the experimental validation of the prototype component was carried out at the test facility of the *Politecnico di Milano University*.

2. Methodology

First of all the main characteristics and features of the PVT technology were analyzed and implemented in a prototype of covered hybrid collector. At the second stage a simulation model of the PVT collector was developed through the elaboration of several mathematical equations. The model is able to calculate the electrical and thermal performance of the PVT collector connected to a storage tank, as a function of inputs related to climatic and real operating conditions.

Subsequently, a monitoring campaign data on the experimental collector placed at the test facility of the *Politecnico di Milano* was carried out and the model validation is presented.

Finally, considerations about daily and annual yield of the PVT collector compared to a traditional photovoltaic module are discussed.

3. Design of the PVT collector and prototype equipment

In order to overcome the well-known temperature effect (Skoplaki and Palyvos, 2009; Kurnik et al., 2011) that is decisive in the characterization of the electrical performance of a PVT module, the developed PVT collector integrates a silicon thin film double junction sandwich characterized by a low temperature coefficient. This technology allows to reduce temperature power losses, which are generally higher in PVT systems than in PV modules. Moreover, when subjected to high temperatures, modules with a junction of a-Si undergo a sort of regeneration process, called thermal annealing, which increases the electrical efficiency (initially lost due to the Staebler–Wronski effect). In detail the adopted technology combines an amorphous silicon top layer and a microcrystalline silicon layer (a-Si/μc-Si). The top cells absorb and convert the visible solar spectrum, while the bottom one is sensitive to near infrared wavelengths. The electrical features of the adopted PV sandwich are reported in the following table.

The PV sandwich was bonded mechanically with two roll-bond aluminum absorbers with channels arrangement reported in Fig. 1. This type of absorber is one of those characterized by the best performance in PVT applications. Parallel pipe configuration, as known (Weitbrecht et al., 2002; Pieper and Klein, 2011; Aste et al., 2014) ensures slow temperature gradients between input and output and good temperature distribution on the whole absorber surface, with electrical and thermal benefits on PVT collec-tor efficiency. Moreover, in order to obtain a better flow distribution in the channels, an optimized layout of the header manifolds was chosen according to the PVT state of the art (Aste et al., 2014).

It has to be noted that the most advanced technique for the connection between PV section and the absorber is the lamination of the whole package (Glass, PV cells, electrical insulation and absorber) in one step (Dupeyrat et al., 2009). However, at the experimental stage, that technique was valuated too expensive and difficult to realize; the prototype was thus built with a commercial glass–glass PV module bonded with the absorber.

Furthermore, as already said, modules with at least a layer of a-Si, if subjected to extended exposure to high temperatures, are able to recover some or all of their initial electrical performance (Del Cueto and von Roedern, 1999; Gottschalg et al., 2003; Jansen et al., 2006; Pathak et al., 2012; Virtuani and Fanni, 2014). As a consequence, in order to increase the output fluid temperature and so the

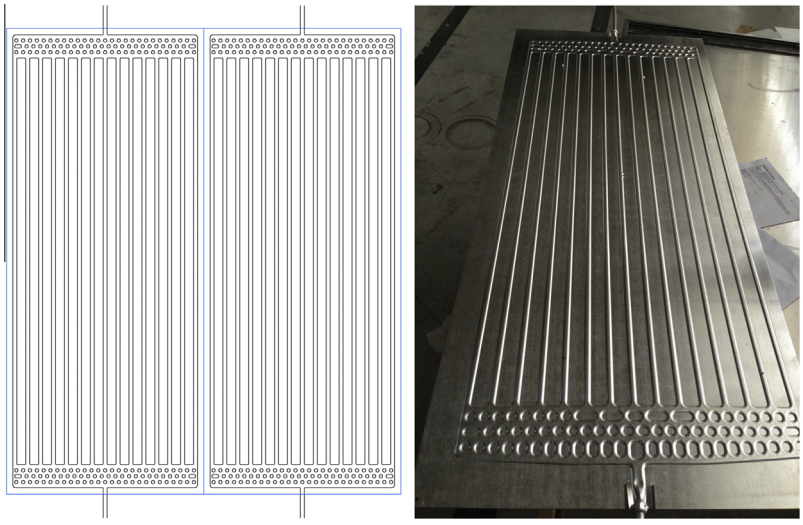

Fig. 1. Absorber configuration.

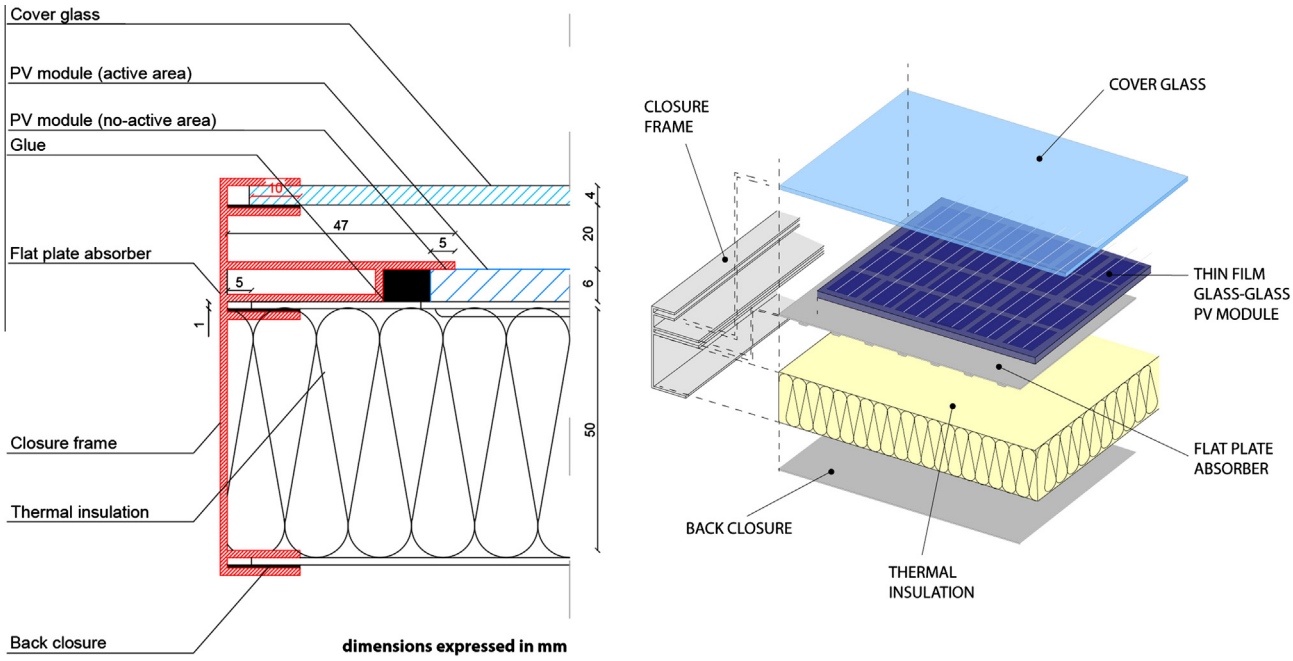

Fig. 2. Section and isometric view of the stratification of the collector.

Table 1
PVT and PV electrical parameters.

Parameter	Value	Unit
Nominal power	125	W
V_{mpp}	56.6	V
I_{mpp}	2.21	A
V_{oc}	74.1	V
I_{sc}	2.71	A
Temperature coefficient on power	−0.25	%/K

electrical production, the components are enclosed into an aluminum frame and covered by a glass 4 mm thick; the air gap between the PV laminate and the glass cover is 20 mm depth. Also in this case, an insulated PV sandwich with the air gap could be directly made similarly to a double-glazing, avoiding the interposition of two separated glasses above PV cells (Dupeyrat et al., 2011), but in the experimental stage such solution was considered too complex. For such reason, the experimental prototype was made with two glasses: the cover one and the one contained in the PV sandwich. Of course the presence of two glasses increases the optical losses. Moreover a thermal insulation of mineral fiber mat material, 50 mm thick, applied in the rear side of the absorber, further reduces thermal losses. A representation of the PVT collector is shown in Fig. 2 and the main features are summarized in Table 2. The featured quantities were provided by experimental measurement, by technical data sheets or are values widely used in literature for similar systems.

The PVT collector was connected to a cylindrical storage tank and a forced circulation system with flow loop between PVT solar collector and tank was assumed for this study. A water pump at the inlet of the collector is used to transfer hot water to the upper part of the storage tank. The lower density of the hot water causes stratification in the tank (Ievers and Lin, 2009), improving thermal efficiency and avoiding overheating of the photovoltaic cells.

4. Considerations about PV efficiency

The nominal efficiency of PV cells is a parameter measured at Standard Test Conditions (STC), with cells temperature of 25 °C, normal irradiance of 1000 W/m^2 and a solar spectrum corresponding to Air Mass (AM) of 1.5.

However, the real operating conditions can be remarkably different from those of reference, influencing meaningfully the performance and therefore the electric power production. For these reasons it is useful to define the value of real efficiency (η_a), taking into account variations of operative temperature of the cells, incident angle of solar irradiance and solar spectrum, related as follows (Aste and Del Pero, 2006):

$$\eta_a = \eta_n \times k_\gamma \times k_\theta \times k_\lambda \times k_g \quad (1)$$

where η_n is the nominal efficiency of the PV module, k_γ is the module temperature correction factor, function of the PV power temperature coefficient γ_{PV}, given by:

$$k_\gamma = [1 - \gamma_{PV} \times (T_{PV} - 298.15)] \quad (2)$$

k_θ is the optical reflection correction factor, defined as the ratio between the solar transmittance at specific angle of incidence on the front cover surface, calculated according Fresnel formula, and the corresponding value at normal incidence, given by:

Table 2
Main reference parameters.

Parameter	Symbol	Value	Unit
Front cover			
Glass thickness	δ_G	0.004	m
Depth of air gap underneath	H	0.02	m
Glass thermal capacity	C_G	840	J/(kg K)
Solar transmittance at normal incident angle	t_n	0.9	–
Solar absorbance of glass	α_G	0.1	–
Far infrared emissivity of the glass	ε_G	0.88	–
Density of the glass	ρ_G	2500	kg/m^3
Sky view factor	F	0.93	–
PV sandwich			–
Nominal power	P_n	125	W_p
Nominal efficiency	η_n	8.9	%
Power temperature coefficient	γ_{PV}	−0.25	%/K
Thickness	δ_{PV}	0.006	m
Solar absorbance of the PV sandwich	α_{PV}	0.9	–
Far infrared emissivity of the PV sandwich	ε_{PV}	0.9	–
Packing factor	p	0.98	–
Density of the PV sandwich	ρ_G	2500	kg/m^3
PV sandwich thermal capacity	C_{PV}	840	J/(kg K)
PV thermal absorber			
Length	–	1.3	m
Width	–	1.1	m
Number of pipes	n	30	–
Pipe distance	–	0.02	m
Pipe length	L	1.26	m
Pipe cross section area	–	0.000014	m^2
Thermal insulation			
Thickness	–	0.05	m
Conductivity	–	0.035	W/m K
Storage system			
Mass of water in tank	M_w	200	kg
Water thermal capacity	C_w	4186	J/(kg K)
External area of the storage tank	S_{tk}	5.16	m^2
Heat loss coefficient of the storage tank	U_{tk}	5	W/m^2 K

$$k_\theta = \frac{\tau_G}{\tau_n} \tag{3}$$

k_λ is the spectrum correction factor, function of the actual spectrum of the solar radiation on the collectors surface respect of that measured at STC.

In thin film modules, such as the PV laminate adopted in the prototype, k_λ can be calculated using an empiric formula which relates the changes of incident solar light spectrum to AM (Riordan and Hulstron, 1990) to characterize the influence of spectral variation on the production of the PV sandwich (Hecktheuer, 2001):

$$k_\lambda = 1.0547 - 0.0214 \times \mathrm{AM} - 0.0075 \times \mathrm{AM}^2 + 0.0004 \times \mathrm{AM}^3 \tag{4}$$

k_g is the low irradiance correction factor, in order to take into account the power losses due to low irradiance behavior of PV modules. It is important to note that in some technologies, such as micromorphous cells, the low irradiance behavior, in particular below 200 W/m^2, is counterbalanced by a higher performance due to the greater share of diffuse radiation (Belluardo et al., 2012).

In the following mathematical set of equations all the above factors will be considered for the determination of electrical performance.

A useful parameter for the simulation model further considered is the so-called thermal–spectral efficiency, which represents the variation of η_n in operating conditions due to actual temperature of the cells and solar spectrum only. It can be expressed as follows:

$$\eta^* = \eta_n \times k_\gamma \times k_r\lambda \times k_g \tag{5}$$

It is important to note, as already mentioned, that an amorphous silicon cell subject to high temperatures (from 50 °C to 100 °C), undergoes a sort of regeneration process, which increases the electrical efficiency (initially lost due to the Staebler–Wronski effect). That regeneration, known as thermal annealing, can increase the electrical production of the PVT component up to 10% (Pathak et al., 2012). However, thermal annealing has not been yet translated into an analytical formula, for that reason the proposed following model does not take into account this effect. Nevertheless, the experimental outdoor validation campaign was con-

ducted during winter and the cells' temperature did not reach values over 25 °C, so regeneration effect did not take place.

5. Simulation model

The developed simulation model is based on energy balances of the different components of the PVT system including the cylindrical storage tank, solved at any desired time step. The model takes in consideration also the thermal inertia of main subcomponents.

The model consists in 5 balance equations of the collector sub-systems (glass cover, PV cells, air gap and absorber plate), 2 equations related to the storage tank and 5 equations for the dynamic calculation of convective and radiative coefficients.

The energy balance equations are organized in a numerical matrix, whereas the radiative coefficient equations are solved by means of an iterative procedure.

In order to define the thermal balance of the PVT collector, the whole PV sandwich and the absorber, hereafter identified as the PV absorber, were considered at the same temperature of the cells. This hypothesis is reasonable, since the lamination glasses have a very small thickness.

5.1. Thermal balance of the glass

The thermal balance of the glass is calculated assuming that the radiation absorbed from the glass is equal to the energy accumulated from the glass and the external and internal energy losses.

$$(I_t \times S_G \times \alpha_G) = \rho_G \times \delta_G \times S_G \times C_G \times \frac{dT_G}{dt} + h_e \times S_G \times (T_G - T_e) + h_{ic} \times S_G \times (T_G - T_{ma}) + h_{rG-PV} \times S_G \times (T_G - T_{PV}) \quad (6)$$

where I_t is solar irradiance on the collector (W/m^2); S_G is the area of the cover glass (m^2); α_G is the solar absorbance of glass; ρ_G, δ_G, S_G, C_G, are respectively the density, thickness, surface area and heat capacity of the glass; T_G is the temperature of the glass (K); dt is the time step of the dynamic simulation (s); h_e is the external convective and radiative coefficient of glass cover (W/m^2 K); T_e is the ambient air temperature (K); h_{ic} is the convective coefficient of the air gap (W/m^2 K); T_{ma} is the average temperature of the air gap (K); h_{rG-PV} is the glass–PV radiative heat transfer coefficient; T_{PV} is the temperature of the PV cells (K).

5.2. Thermal balance of the PV sandwich

The thermal balance of the PV sandwich is calculated assuming that the radiation absorbed from the PV sandwich is equal to the accumulated thermal energy, the electricity produced by the cells, the energy transferred from the PV sandwich to the absorber and then to the heat transfer fluid, the convective losses in the air gap, the radiative exchange between PV cells and glass cover and the conductive thermal losses.

$$(I_t \times S_G \times \tau_G \times \alpha_{PV}) = S_{PV-a} \times \rho_{PV} \times \delta_{PV} \times C_{PV} \times \frac{dT_{PV}}{dt} + \left(I_t \times \tau_G \times p \times S_{PV-a} \times \frac{\eta^*}{\tau_n}\right) + h_w \times S_{PV-a} \times (T_{PV} - T_{mw}) + h_{ic} \times S_{PV-a} \times (T_{PV} - T_{ma}) + h_{rG-PV} \times S_{PV-a} \times (T_{PV} - T_G) + U_F \times S_{PV-a} \times (T_{PV} - T_e) \quad (7)$$

where I_t is solar irradiance on the collector (W/m^2); S_G is the area of the cover glass (m^2); τ_G is the solar transmittance of the glass, dependent on incident angle; α_{PV} is the solar absorbance of PV sandwich; S_{PV-a} is the surface area of the PV absorber (m^2); ρ_{PV}, δ_{PV}, C_{PV}, are respectively the density, thickness and heat capacity of the PV sandwich; T_{PV} is the temperature of the PV (K); dt is the time step of the dynamic simulation (s); p is the packing factor of the module; η^* represents the thermal–spectral efficiency of the PV module; τ_n is the solar transmittance of the glass, at normal incident angle; h_w is the heat transfer coefficient of the heat exchanger (W/m^2 K); T_{mw} is the average temperature of the water in the heat exchanger (K); h_{ic} is the convective heat transfer coefficient of the air enclose in the gap (W/m^2 K); T_{ma} is the average temperature of the air gap (K); h_{rG-PV} is the glass–PV radiative heat transfer coefficient (W/m^2 K); U_F is lateral and back heat loss coefficient of the collector (W/m^2 K); T_e is the ambient air temperature (K).

5.3. Water in channels

The thermal balance of the water in the absorber is calculated considering that the sum of the thermal energy coming out from the collector and the energy accumulated by the fluid in channels is equal to the energy transferred from the PV absorber to water.

$$\dot{m}_w \times C_w \times (T_{out} - T_{in}) + \rho_w \times S_S \times C_w \times L \times n \frac{dT_{mw}}{dt} = h_w \times S_{PV-a} \times (T_{PV} - T_{mw}) \quad (8)$$

where $\dot{m}_w$ is the mass flow rate of the water inside the absorber (kg/s); C_w is the heat capacity of the water (J/kg K); T_{out} is the temperature of the water at outlet (K); T_{in} is the inlet fluid temperature (K); ρ_w is the density of the water inside the channel (kg/m^3); S_S is the cross-section area of each channel (m^2); L is the length of the channel (m); n is the number of channels in the plate; h_w is heat transfer coefficient of the water in the absorber (W/m^2 K); S_{PV-a} is the surface area of the absorber (m^2); T_{PV} is the temperature of the PV sandwich (K); T_{mw} is the average temperature of the water in the absorber (K).

5.4. Mean fluid temperature

The mean fluid temperature is calculated as the average between fluid temperatures at inlet and outlet of the collector.

$$T_{\mathrm{mw}} = \frac{T_{\mathrm{out}} + T_{\mathrm{in}}}{2} \tag{9}$$

where T_{in} is the inlet fluid temperature (K) and the T_{out} is the temperature of the fluid at the outlet of the hybrid collector (K).

5.5. Mean air temperature in the air gap

The mean air temperature in the gap is calculated with a simplified formula as the average temperature between PV sandwich and the glass cover.

$$T_{\mathrm{ma}} = \frac{T_G + T_{\mathrm{PV}}}{2} \tag{10}$$

where T_G is the glass cover temperature (K) *e* T_{PV} is the temperature of the PV sandwich (K).

5.6. Water in the storage tank

Thermal balance of the water in the storage tank is described as follow:

$$M_w \times C_w \times \frac{dT_{\mathrm{tk}}}{dt} = \dot{m}_w \times C_w \times (T_{\mathrm{tk,i}} - T_{\mathrm{tk,o}}) + U_{\mathrm{tk}} \times S_{\mathrm{tk}} \times (T_e - T_{\mathrm{tk}}) \tag{11}$$

where M_w and C_w, are respectively the mass (kg) and the heat capacity (J/kg K) of the water in storage tank; T_{tk} is the mean fluid temperature in the tank (K); $T_{\mathrm{tk,i}}$ is the temperature of the water at inlet of the tank (K); $T_{\mathrm{tk,o}}$ is the temperature of the water at outlet of the tank (K); U_{tk} is the heat loss coefficient at the outside surface of the tank (W/m^2 K).

It is possible to consider, with a negligible error, that the mean fluid temperature of the storage tank is equal to the average temperature of the water at inlet and at outlet of the tank.

$$T_{\mathrm{tk}} = \frac{T_{\mathrm{tk,i}} + T_{\mathrm{tk,o}}}{2} \tag{12}$$

5.7. Thermal exchange coefficient

The external convective and radiative heat transfer coefficients depend on the average temperatures, $T_{\mathrm{G-sky}}$, $T_{\mathrm{G-PV}}$, described below. For the determination of the relevant heat transfer coefficients, the simulation model employs an iterative procedure to obtain the values of these temperatures.

In detail the external convective and radiative coefficient of glass cover is calculated as illustrated hereafter.

$$h_e = h_v + h_{\mathrm{rG-sky}} \tag{13}$$

where h_e (W/m^2 K) is the external radiative and convective heat transfer coefficient; h_v (W/m^2 K) is the external convective coefficient, calculated with the (14) (Watmuff et al., 1977); $h_{\mathrm{rG-sky}}$ (W/m^2 K) is the external radiative heat transfer coefficient between glass cover and sky (15).

$$h_v = 2.8 + 3 \times w_e \tag{14}$$

where w_e (m/s) is the wind velocity.

$$h_{\mathrm{rG-sky}} = F \times 4 \times \varepsilon_G \times \sigma \times T^3_{\mathrm{G-sky}} \tag{15}$$

where F is the sky view factor of the collector; ε_G is the infrared emissivity of the glass cover; σ is the Stefan–Boltzmann constant equal to 5.67×10^{-8} W/m^2 K^4; $T_{\mathrm{G-sky}}$ is the average glass cover–sky temperature (K) expressed as:

$$T_{\mathrm{G-sky}} = \frac{T_G + T_{\mathrm{sky}}}{2} \tag{16}$$

where T_{sky} is the equivalent radiative temperature of the sky (K) and can be expressed by the following linear equation (Unsworth and Monteith, 1975):

$$T_{\mathrm{sky}} = 0.0552 \times T_e^{1.5} + 2.625 \times N \tag{17}$$

where T_e is the ambient temperature (K); N is the sky cloud coverage in octaves.

The glass–PV sandwich radiative coefficient $h_{\mathrm{rG-PV}}$ is calculated by the following equation:

$$h_{\mathrm{rG-PV}} = 4 \times \varepsilon_{\mathrm{G-PV}} \times \sigma \times T^3_{\mathrm{ma}} \tag{18}$$

where $\varepsilon_{\mathrm{G-PV}}$ is the equivalent glass–PV sandwich infrared emissivity and can be written as follows:

$$\varepsilon_{\mathrm{G-PV}} = \frac{1}{\frac{1}{\varepsilon_G} + \frac{1}{\varepsilon_{\mathrm{PV}}} - 1} \tag{19}$$

T_{ma} is the average air temperature in the gap in Kelvin (10).

The convective heat transfer coefficient of the air enclose in the gap (h_{ic}) (W/m^2 K) is related with the air thermal conductivity (λ) equal to 0.024 W/m K, Nusselt number (Nu) and thickness of air gap (H) (m) by the following expression:

$$h_{\mathrm{ic}} = \frac{\mathrm{Nu} \times \lambda}{H} \tag{20}$$

For tilt angles ranging from 0° to 75°, Hollands et al. (1976) presented an equation in order to calculate the Nusselt (Nu) number, as function of the Raleigh (Ra) number as follows:

$$\mathrm{Nu} = 1 + 1.14 \left(1 - \frac{1708 \cdot (\sin 1.8\theta)^{1.6}}{\mathrm{Ra} \cdot \cos\theta}\right) \times \left[1 - \frac{1708}{\mathrm{Ra} \cdot \cos\theta}\right]^{+} + \left[\left(\frac{\mathrm{Ra} \cdot \cos\theta}{5830}\right)^{1/3} - 1\right]^{+} \tag{21}$$

where the + exponent indicates that only positive value for terms within the square brackets have to be used. In case of negative values, zero is used. Raleigh number is calculated as follows:

$$\mathrm{Ra} = \frac{g \times \beta \times (T_{\mathrm{PV}} - T_G) \times H^3}{v \times \varphi} \tag{22}$$

where g is the acceleration due to gravity (m/s^2), β is the thermal expansion coefficient (K^{-1}), T_G is the glass cover temperature (K) *e* T_{PV} is the temperature of the PV sandwich (K), H is the thickness of air gap (m), v and φ are respectively the kinematic viscosity (m^2/s) and the thermal diffusivity of air (m^2/s).

6. Prototype installation and monitoring campaign

In order to evaluate the accuracy of the simulation model, an experimental monitoring campaign on the prototype PVT collector was performed from 14/12/2013 and interrupted on 24/12/2013 in order to avoid water freezing. The collector was installed at the experimental station of the *Politecnico di Milano*, as shown in Fig. 3, with tilt angle of 30° and azimuth equal to 0°.

The flow rate of the circulation water has been set at 0.066 kg/s, according to pump size. It is useful to note that at experimental stage, the electrical consumption of the circulation pump was not considered, as it is function of pump type and efficiency. In any case, the pressure drop of the entire system at the given flow rate is 200 mbar; so, considering an high-efficiency circulation pump, the electrical power necessary to maintain a constant flow rate was set equal to 1.7 W, which can be considered a negligible value.

The PVT collector was connected to an insulated storage tank with capacity of 200 l.

A real time monitoring system, schematized in Fig. 4, has been connected to the PVT system in order to measure thermal and electrical performance. The data monitoring system consists of the following equipment:

- 2 solar irradiance sensors, installed with the same tilt and azimuth angle of the collector, to measure the global solar irradiance on the collector's plane;

Fig. 3. PVT system placed at Politecnico di Milano.

- 1 temperature sensor (PT 100) positioned between the absorber plate and the insulating material, measuring the temperatures of the PV absorber;
- 2 immersion temperature sensors, placed at the inlet and outlet of the PVT collector, to measure the inlet and outlet temperatures of the fluid;
- 2 pressure gauges, to measure the pressure drop of the channel in the PVT heat exchanger;
- 1 meteorological station installed nearby the system to measure direct and diffuse solar radiation on horizontal plane and ambient air temperature;
- voltage and current sensors connected to the DC/AC inverter.

The DC/AC conversion is operated by a single phase transformerless micro-inverter with MPPT tracker. The efficiency curve of the inverter provided by the manufacturer was verified with an experimental data-acquisition campaign performed on the described PV module. The obtained data are shown in Fig. 5.

Since the monitoring system acquires the output electrical power in AC, the calculated power from the model is implemented as a function of the real efficiency curve of the inverter.

As it can be noted in Fig. 3, in order to evaluate the difference, in terms of energy efficiency, between PVT and PV technologies, a standard photovoltaic sandwich with the same geometrical and electrical features of the one integrated in the PVT collector was installed and monitored. The results are shown in Section 9.

It has be noted that, since the performance of the modules cells in a-Si is strongly influenced by Staebler–Wronski effect (Stabler and Wronski, 1977), at the first step both PV laminates (the one inside the PVT collector and the standard PV module) were exposed and monitored for two months (June and July). Fig. 6 shows the degradation process as function of the daily performance ratio on energy (PR) in %, defined as follows:

$$\mathrm{PR}_d = \frac{E}{\frac{G}{1000} \times P_n} \tag{23}$$

where E is the energy generated in direct current during a day (W h), G is the daily solar irradiation on the PV module (W h/m^2 day) and P_n (W) is the nominal power of the module measured at STC.

As shown, the degradation process leads to a decrease in module performances of about 10%; that effect is noticeable during the first 20/30 days of sun exposure, while reaches a stabilized performance during the remaining time. It is important to note that the stabilization process was carried out in both modules with the same results.

Note that the stabilization level depends on different combinations of irradiance level and module temperature during the process (Kenny et al., 2014).

After the stabilization period, the reported monitor campaign was performed.

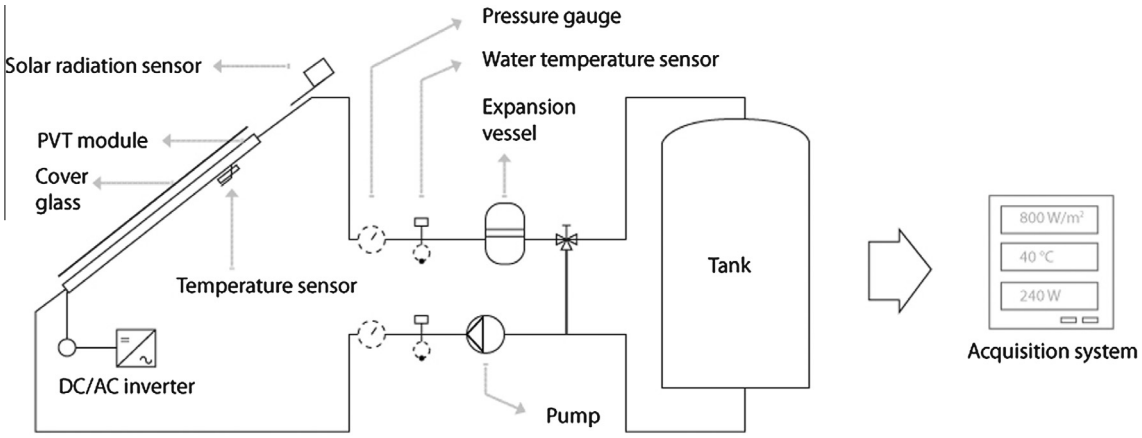

Fig. 4. PVT monitoring system.

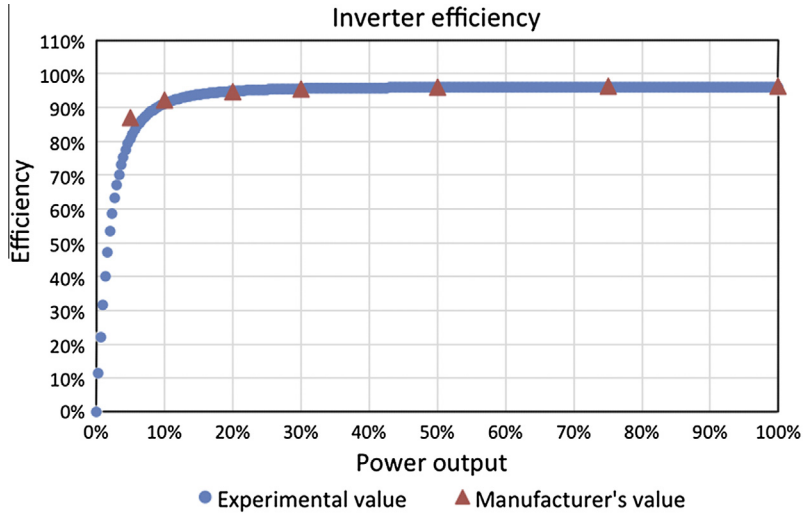

Fig. 5. Micro-inverter efficiency curve.

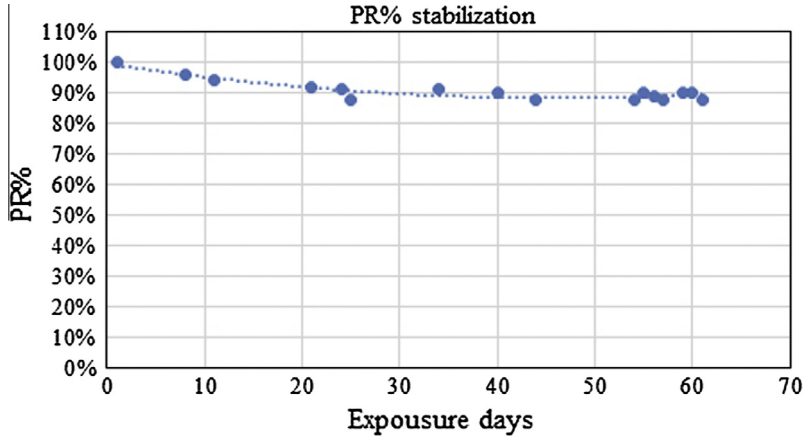

Fig. 6. Staebler–Wronski effect.

7. Experimental data and performance simulation

The proposed simulation model was implemented in a spreadsheet and performance simulations were carried out for the monitored days, from 14/12/2013 to 24/12/2013, from 7:30 to 16:00 (real solar hour) with a time step of 15 min. The inputs of the simulation model, such as irradiance on the collector plane, ambient temperature, water temperature in the tank when the system starts and water flow rate, were set according to experimental data collected

from the monitoring acquisition. The sky cloud coverage is calculated according to a visual analysis provided by a fish-eye camera installed in the facility. In Fig. 7, samples of clear and overcast sky conditions are shown.

It must be specified that the adopted immersion temperature sensors are able to measure temperatures from 10 °C to 90 °C, because it has no sense to consider lower values as the water from the supply network in Milan has always a temperature greater than 10 °C. Anyway, since the test facility is placed outdoor and the monitoring campaign was carried out during the winter, in some cases the water temperature in the tank decreased slightly below 10 °C during the night; for such reasons, simulations on electrical and thermal productivities were carried out and compared to experimental data just when water temperatures were greater than 10 °C.

Moreover, despite a-Si and a-Si/μ-Si cells have better performances than c-Si at low irradiance (Belluardo et al., 2012), it must be noted that the electricity production during very cloudy days was about equal zero. In fact, under overcast conditions, the PV output is very low, and therefore, the inverter operates at low-power-input conditions. In such situations, the inverter cannot start converting DC to AC until the input power reaches a minimum threshold level (Mondol et al., 2006).

A general overview of the simulated and monitored electrical and thermal energy productions of the PVT module was reported in Fig. 8 and analyzed more in detail in Section 8.

The difference between measured and calculated data can be attributed mainly to the accuracy of the sensors and in some inaccuracies in the data provided by manufacturers, as explained in detail below in the paper.

8. Model validation and error analysis

The numerical model was validated by comparing in detail the simulation results with measured data collected during four sample-days, chosen among monitored days as they well represent the average characteristics of two different climatic conditions: almost clear sky condition (14st–16st December 2013) and scattered cloudy sky condition (15st–18st December).

In detail, in order to compare experimental and calculated data, electrical power and inlet/outlet water temperature of the PVT collector are shown in Figs. 9 and 10 for two representative sample days.

As it can be seen in Fig. 8 the performance drop is related to the irradiance decreasing due to a momentary presence of a cloud. The decreasing in irradiance has been considered particularly useful for the validation of the model.

From Figs. 9 and 10 it can be observed that there is a quite good agreement between measured values and those calculated by the simulation model even if the solar irradiance changes quickly.

It is important to note that, in order to avoid the temperature's drop of the water in the tank, particularly in the last hours of the day, the circulation pump is switched off when the temperature of the outlet water flow from the collector starts to be equal to the water temperature of the inlet flow.

Despite the solar radiation has a variable trend over time, the predicted output power obtained from the simulation model fits quite well with the real data. To compare the results of the calculations with the experimental measurements, the correlation coefficient (r) and root mean square percent deviation (e) have been evaluated by using the following expressions.

$$r = \frac{N\sum X_i Y_i - (\sum X_i)(\sum Y_i)}{\sqrt{N\sum X_i^2 - (\sum X_i)^2}\sqrt{N\sum Y_i^2 - (\sum Y_i)^2}} \tag{24}$$

$$e = \sqrt{\frac{\sum (e_i)^2}{N}} = \sqrt{\frac{\sum \left(\left[\frac{X_i - Y_i}{X_i}\right] \times 100\right)^2}{N}} \tag{25}$$

where X_i are theoretical values, Y_i experimental values and N the number of values.

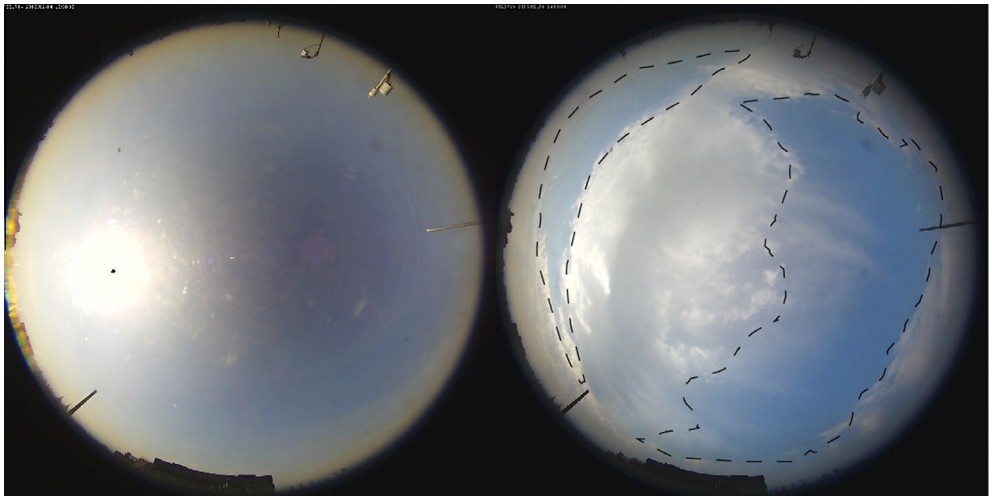

Fig. 7. Fish eye views of clear ($N = 0$) and overcast sky conditions ($N = 4$).

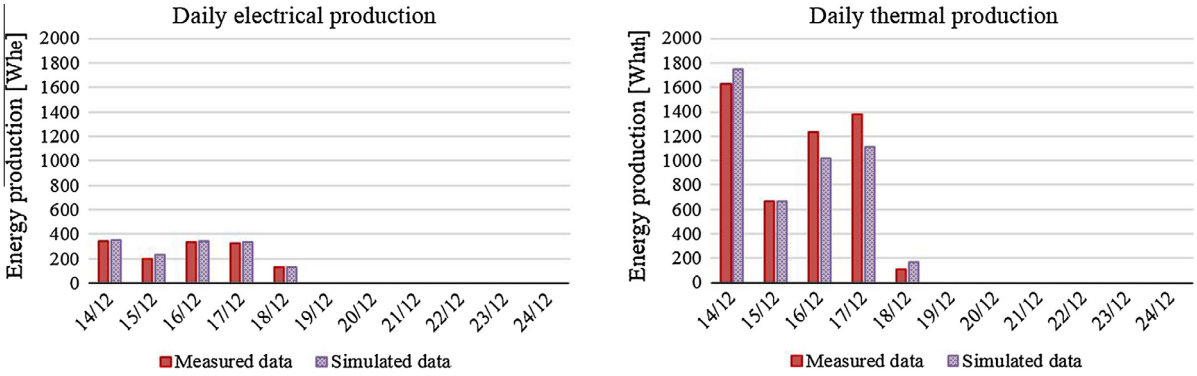

Fig. 8. Electrical and thermal production in analyzed days.

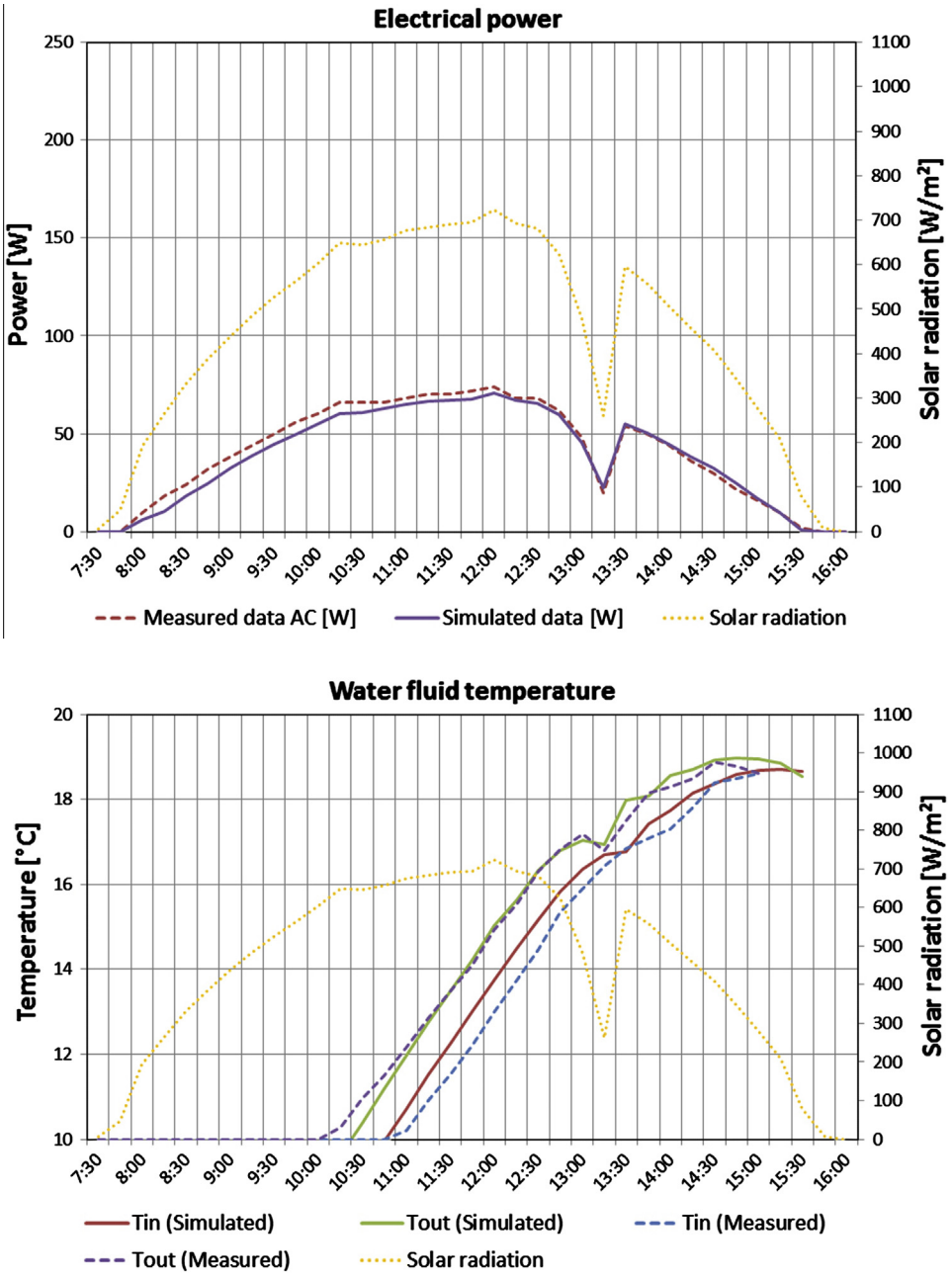

Fig. 9. Measured and calculated data – December 14th 2013.

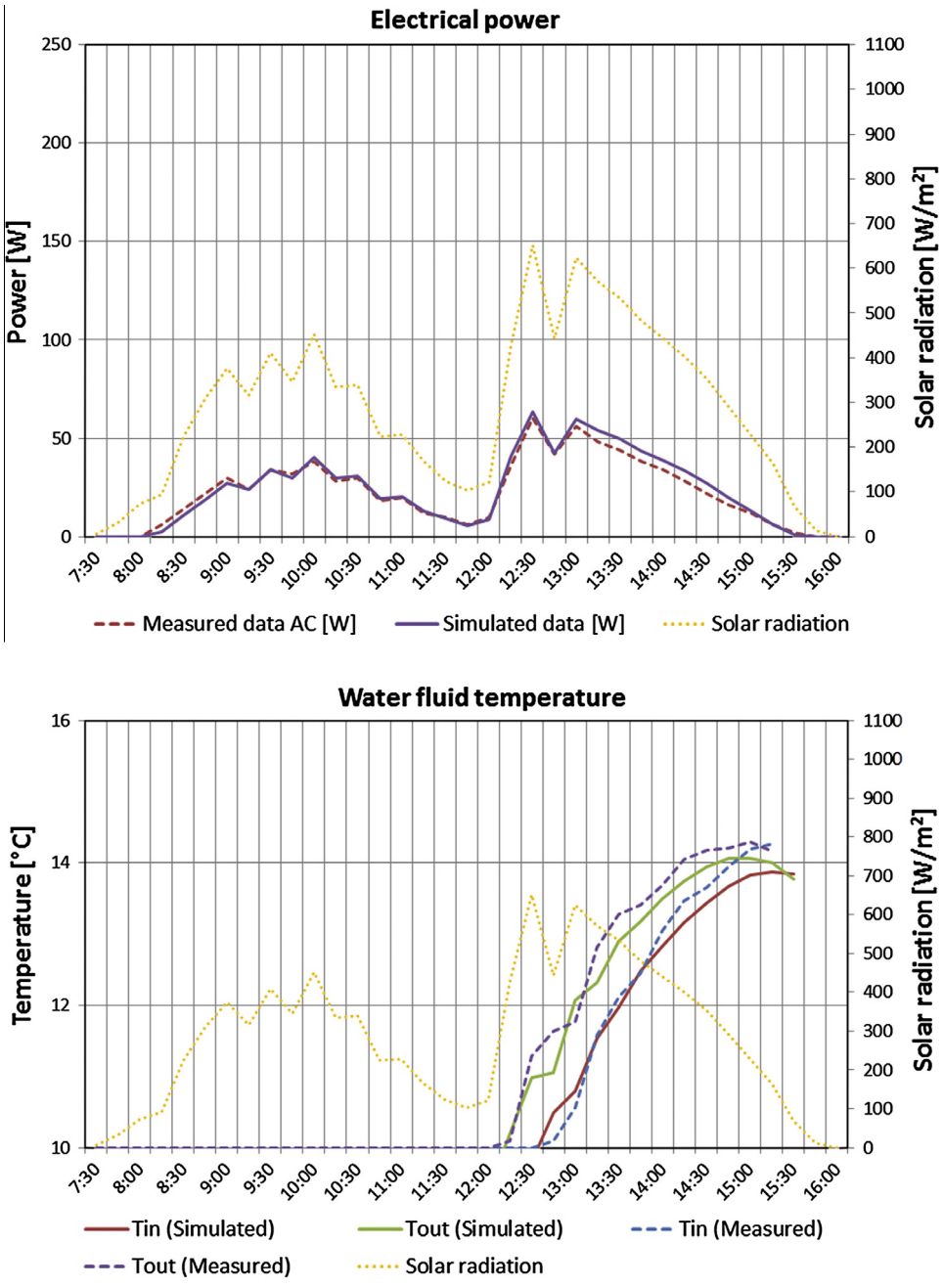

Fig. 10. Measured and calculated data – December 15th 2013.

The results of four analyzed days are reported in Table 3.

It should be noted that, among all parameters used in the calculation model, the peak power of the module is the one that can be considered affected by a significant uncertainty; in fact the manufacturer usually declares that the stabilized power is equal to the nominal value ± certain percentage. In this sense, a sensitivity analysis was carried out on the model in the analyzed clear days, introducing a variation of ±3% on the nominal powers (and thus efficiencies), according to the values specified by the manufacturer of the considered PV module. Related results were reported in Table 4.

As it can be noted from obtained results, the introduced variation on module efficiency has a low influence both on correlation coefficient (r) and on root mean square percent deviation (e).

It must be noted that relative uncertainty on measured data can be obtained by calculating the fractional or absolute uncertainties, according to specifications of measuring instruments, which are the following:

- Solar irradiance, acquired by a solarimeter equipped with a photodiode sensor: ±4%.
- Electrical power, acquired by voltage and current sensors: ±1%.

Table 3
Validation results.

		Experimental (mean daily value)	Theoretical (mean daily value)	r	e (%)
Clear days	Power AC	25.62 W	24.71 W	0.989	15.36
	T_{in} (°C)	15.45 °C	15.20 °C	0.943	4.86
	T_{out} (°C)	15.83 °C	15.56 °C	0.938	5.03
Cloudy days	Power AC (W)	12.16 W	12.77 W	0.995	14.97
	T_{in} (°C)	11.86 °C	11.56 °C	0.978	4.40
	T_{out} (°C)	11.93 °C	11.74 °C	0.966	4.38

Table 4
Validation results (clear days).

		Experimental (mean daily value)	Theoretical (mean daily value)	r	e (%)
Clear days $\eta_n + 3\%$	Power AC	25.62 W	25.35 W	0.989	14.52
	T_{in} (°C)	15.45 °C	15.37 °C	0.956	3.63
	T_{out} (°C)	15.83 °C	15.74 °C	0.925	3.44
Clear days $\eta_n - 3\%$	Power AC	25.62 W	23.87 W	0.989	16.83
	T_{in} (°C)	15.45 °C	15.42 °C	0.941	3.62
	T_{out} (°C)	15.83 °C	15.78 °C	0.928	3.35

- Module and water temperature, measured by PT100 sensor: ±3%.

9. Energy efficiency assessment

As previously reported, in order to evaluate the convenience, in terms of energy, of the designed PVT collector related to a standard PV module, the two technologies with the same electrical characteristics, which are summarized in Table 1, are investigated.

In Fig. 11 the two modules were analyzed in terms of performance ratio on power, which measures the deviation between the actual performances of the PV systems and those theoretically achievable at the Standard Test Condition (STC). It is defined as:

$$\mathrm{PR}_i = \frac{P_i}{\frac{I_t}{1000} \times P_n} \tag{26}$$

where P_i (W) is the output power generated by the module, I_t is the solar irradiance on the module plane (W/m^2) and P_n (W) is the nominal power of the module measured at STC.

Above-mentioned results show that, despite the temperature of the PV module is higher than the one of the PV sandwich inside the hybrid collector, the performance ratio

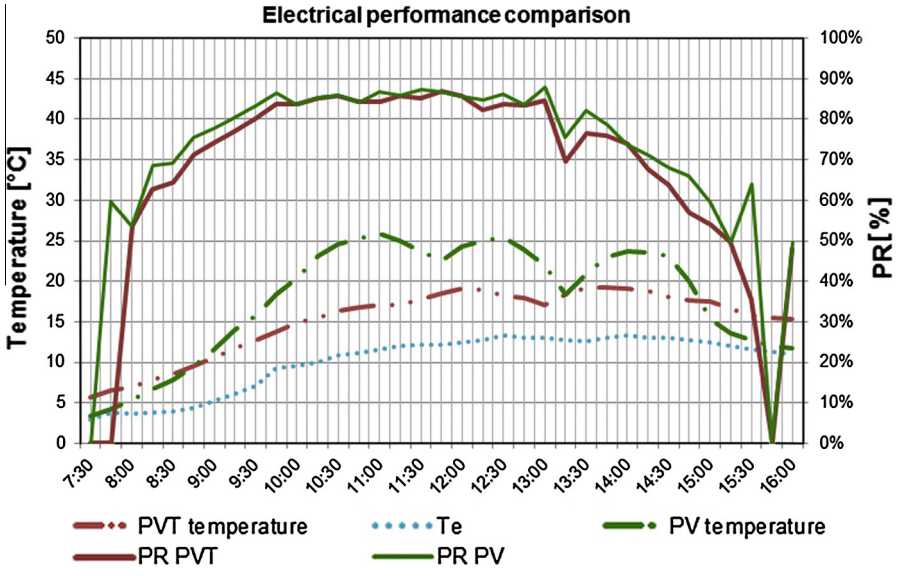

Fig. 11. PR comparison – December 14th 2013.

of the standard PV system is slightly higher than that of the PVT. In fact, as previously reported, the experimental PVT component has more reflection losses due to the cover glass compared to the PV module.

In detail the daily mean electrical efficiency of the PVT is 6.0% while the PV module has a daily average efficiency of 6.2%. However, in the analyzed day, the PVT collector was able to produce thermal energy with a daily efficiency equal to 25.8%.

In order to evaluate the annual performance of the two solar technologies in terms of primary energy, a simulation was performed with the model described above, considering for the standard PV module just equations related to electricity production. The results are expressed in terms of primary energy efficiency (η_{PES}) (Huang et al., 2001), a useful parameter that allows comparing electricity with thermal energy. It was valuated as follows:

$$\eta_{PES} = \eta_{th} + \frac{\eta_a}{\eta_{Tpower}} \tag{27}$$

where η_{Tpower} is the average efficiency of power plants at national level. It depends on the manner whereby electric energy is generated in every reference context. A value of 0.46 (AEEG, 2008) corresponds to the typical fuel mix used for electricity production in Italy.

Obtained results showed that the annual primary efficiency of the PV module is equal to 13.4%, while the PVT collector is able to convert solar energy in primary energy with an overall efficiency of 42%, which is given by a 13.2% of electricity (converted in primary energy) and 28.8% of thermal energy. Such results are promising considering that the average annual efficiency of glazed PVT collectors is estimated around 40% (Zondag et al., 2003; Chow et al., 2006, 2007) and the electrical efficiency of the adopted thin film PV module is lower than the one of c-Si modules utilized in several newer PVT components (Dupeyrat et al., 2011). Moreover, it must be underlined that the proposed simulation model does not take in account the positive effect of thermal annealing during the hot seasons, which will be investigated in further steps of the research.

As a final point it is important to note that thermal efficiency is calculated considering that, every morning when the system starts, the water temperature in the tank is equal to 10 °C, which is assumed to be the temperature of the water coming from supply network. However such value can be considered precautionary, corresponding to the minimum temperature of the water in an insulated tank placed inside a building.

10. Conclusions

In the present work the design of an experimental PVT collector and a new dynamic model for the simulation of flat plate PVT water collectors are presented. The proposed model takes into account various terms which influence the performance of hybrid collectors as the spectral efficiency, the loss due to temperature, the real angle of incidence of the solar radiation on the surface and the thermal inertia of the collector.

The model validation, carried out through the use of measured data from experimental analysis, showed that the numerical model has been able to give accurate simulation of the daily thermal and electric performances also in days with different climatic conditions. However, slight differences between data are due to losses along the circuit and to accuracy of the monitoring system. Finally, the comparison between the experimental PVT collector and the standard PV module is discussed. The present work shows that the PVT technology presents an higher overall efficiency than the simple PV module in terms of primary energy. In fact, despite the electricity production of the PVT component is slightly less than the one of the standard PV module, the PVT technology is able to produce, at the same time, also an amount of thermal energy.

Further works must be focused on summer performance of PVT collectors in order to understand the regeneration effect of a-Si/μc-Si due to high temperatures.

References

AEEG, 2008. Delibera EEN 3/08: aggiornamento del fattore di conversione dei kW h in tonnellate equivalenti di petrolio connesso al meccanismo dei titoli di efficienza energetica.

Aste, N., Del Pero, C., 2006. Simulation model for forecast of the energy performance of PV plants. In: Proceedings of ASME ATI Conference, pp. 14–17.

Aste, N., Chiesa, G., Verri, F., 2008. Design, development and performance monitoring of a photovoltaic–thermal (PVT) air collector. Renewable Energy 33, 914–927.

Aste, N., Del Pero, C., Leonforte, F., 2014. Water flat plate PV–thermal collectors: a review. Sol. Energy 102, 98–115.

Belluardo, G., Pichler, M., Moser, D., Nikolaeva-Dimitrova, M., 2012. One-year comparison of different thin film technologies at Bolzano Airport Test Installation. In: Mendez-Vilas, A. (Ed.), Fuelling the Future: Advances in Science and Technologies for Energy Generation, Transmission and Storage. Brown Walker Press, Boca Raton, FL, pp. 229–234.

Chow, T.T., 2010. A review on photovoltaic/thermal hybrid solar technology. Appl. Energy 87, 365–379.

Chow, T.T., He, W., Ji, J., 2006. Hybrid photovoltaic–thermosyphon water heating system for residential application. Sol. Energy 80, 298–306.

Chow, T., He, W., Ji, J., Chan, A., 2007. Performance evaluation of photovoltaic–thermosyphon system for subtropical climate applica-tion. Sol. Energy 81, 123–130.

Chow, T.T., Pei, G., Fong, K.F., Lin, Z., Chan, A.L.S., Ji, J., 2009. Energy and exergy analysis of photovoltaic–thermal collector with and without glass cover. Appl. Energy 86, 310–316.

Del Cueto, J.A., von Roedern, B., 1999. Temperature-induced changes in the performance of amorphous silicon multi-junction modules in controlled light-soaking. Prog. Photovoltaics Res. Appl. 7, 101–112.

Dupeyrat, P., Menezo, C., Hofmann, P., Wirth, H., Kwiatkowski, G., Binesti, D., Rommel, M., 2009. Development of a high performances PV–thermal flat plate collector. In: Proceedings of CISBAT Conference, Lausanne.

Dupeyrat, P., Menezo, C., Rommel, M., Henning, H., 2011. Efficient single glazed flat plate photovoltaic–thermal hybrid collector for domestic hot water system. Sol. Energy 85, 1457–1468.

Fraisse, G., Menezo, C., Johannes, K., 2007. Energy performance of water hybrid PV/T collectors applied to combisystems of Direct Solar Floor type. Sol. Energy 81, 1426–1438.

Gottschalg, R., del Cueto, J., Betts, T.R., Williams, S.R., Infield, D., 2003. Investigating the seasonal performance of amorphous silicon single- and multi-junction modules. In Proceedings of 3rd World Conference on Photovoltaic Energy Conversion, 2. IEEE, pp. 2078–2081.

Heckttheuer, L.A., Krenzinger, A., 2001. The effects on the photovoltaic system response of reflection, spectrum, voltage drop and temperature. In: 17th EPVSEC European Photovoltaic Energy Conference.

Herrando, M., Markides, C.N., Hellgardt, K., 2014. A UK-based assessment of hybrid PV and solar-thermal systems for domestic heating and power: system performance. Appl. Energy 122, 288–309.

Hollands, K., Unny, T., Raithby, G., Konicek, L., 1976. Free convective heat transfer across inclined air layers. J. Heat Transfer 98, 189–193.

Huang, B.J., Lin, T.H., Hung, W.C., Sun, F.S., 2001. Performance evaluation of solar photovoltaic/thermal systems. Sol. Energy 70, 443–448.

Ievers, S., Lin, W., 2009. Numerical simulation of three-dimensional flow dynamics in a hot water storage tank. Appl. Energy 86, 2604–2614.

Jansen, K.W., Kadam, S.B., Groelinger, J.F., 2006. The advantages of amorphous silicon photovoltaic modules in grid-tied systems, vol. 2, pp. 2363–2366.

Kenny, R.P., Chatzipanagi, A.I., Sample, T., 2014. Preconditioning of thin-film PV module technologies for calibration. Prog. Photovoltaics Res. Appl. 22, 166–172.

Kurnik, J., Jankovec, M., Brecl, K., Topic, M., 2011. Outdoor testing of PV module temperature and performance under different mounting and operational conditions. Sol. Energy Mater. Sol. Cells 95, 373–376.

Mondol, J.D., Yohanis, Y., Smyth, M., Norton, B., 2006. Long term performance analysis of a grid connected photovoltaic system in Northern Ireland. Energy Convers. Manage. 47, 2925–2947.

Pathak, M.J.M., Pearce, J.M., Harrison, S.J., 2012. Effects on amorphous silicon photovoltaic performance from high-temperature annealing pulses in photovoltaic thermal hybrid devices. Sol. Energy Mater. Sol. Cells 100, 199–203.

Pieper, M., Klein, P., 2011. A simple and accurate numerical network flow model for bionic micro heat exchangers. Heat Mass Transfer 47, 491–503.

Riordan, C., Hulstron, R., 1990. What is an air mass 1.5 spectrum? [solar cell performance calculations], pp. 1085–1088.

Skoplaki, E., Palyvos, J.A., 2009. On the temperature dependence of photovoltaic module electrical performance: a review of efficiency/power correlations. Sol. Energy 83, 614–624.

Stabler, D., Wronski, C., 1977. Reversible conductivity changes in discharge-produced amorphous Si. Appl. Phys. Lett. 31, 292. Unsworth, M.H., Monteith, J., 1975. Long-wave radiation at the ground I. Angular distribution of incoming radiation. Q. J. R. Meteorol. Soc. 101, 13–24.

Van Helden, W.G.J., Van Zolingen, R.J.C., Zondag, H.A., 2004. PV thermal systems: PV panels supplying renewable electricity and heat. Prog. Photovoltaics Res. Appl. 12, 415–426.

Virtuani, A., Fanni, L., 2014. Seasonal power fluctuations of amorphous silicon thin-film solar modules: distinguishing between different contributions. Prog. Photovoltaics Res. Appl. 22, 208–217.

Watmuff, J., Charters, W., Proctor, D., 1977. Solar and wind induced external coefficients-solar collectors. Cooperation Mediterr. Energie Sol. 1, 56.

Weitbrecht, V., Lehmann, D., Richter, A., 2002. Flow distribution in solar collectors with laminar flow conditions. Sol. Energy 73, 433–441. Zondag, H.A., de Vries, D.W., van Helden, W.G.J., van Zolingen, R.J.C., van Steenhoven, A.A., 2003. The yield of different combined PV–thermal collector designs. Sol. Energy 74, 253–269.